Series solutions for saturated–unsaturated flow in multi-layer unconfined aquifers

Ali A. Ameli *, James R. Craig, Sanders Wong

University of Waterloo, Department of Civil and Environmental Engineering, 200 University Ave. West, Waterloo, ON N2L 3G1, Canada

ABSTRACT

A semi-analytical mesh-free series solution method is presented for modeling regional steady-state sub-surface saturated–unsaturated flow in 2-D geometrically complex homogenous and stratified hill-slope cross sections. Continuous solutions for pressure in the saturated and unsaturated zone are determined iteratively, as is the location of the water table surface. Mass balance is satisfied exactly over the entire domain except along boundaries and interfaces between layers, where errors are in an acceptable range. The solutions are derived and demonstrated on multiple test cases. The errors for specific cases are assessed and discussed.

© 2013 Elsevier Ltd. All rights reserved.

1. Introduction

Modeling of local and regional subsurface flow supports the understanding of regional impacts of human interference and climate change on ground water systems and associated ecosystems [1]. In many cases, both saturated and unsaturated zones must be included in a model to fully describe observed phenomena [2]. In such cases, numerical (rather than analytical) models have generally been used due to the complexity of subsurface flow, which may include non-linear free boundaries, spatially varying material properties with non-linear head dependency, and the presence of geometrically-complex heterogeneity [2–10]. These discrete models are subject to numerical error and their efficiency and accuracy depend upon the resolution of the underlying grid or mesh. Discretization requirements in numerical methods typically contribute to the computational expense of modeling, particularly for free boundary problems where the location of water table is unknown [7,8]. Grid-free (analytical or semi-analytical) methods may be useful for circumventing adaptive mesh and dry cell issues in widely-used numerical software such as MODFLOW [11]. Such models, however, are often limited to geometrically regular and homogenous systems with trivial boundary conditions where the interaction between saturated and unsaturated zones is neglected or overly simplified [12–15]. Recent advances in semi-analytical series solution approaches have relaxed the constraints on geometry by enhancing the traditional method of separation of variables

with a simple numerical algorithm [16–18]. The purpose of the research is to extend these semi-analytical series solution approaches for application to regional 2-D steady free boundary saturated–unsaturated subsurface flow induced by spatially variable surface fluxes in geometrically complex homogenous and stratified hillslopes.

2. Background

Semi-analytical methods can be used to accurately tackle complex problems by benefiting from the strength of both analytical and numerical algorithms. For linear or linearized problems, methods such as the series approach used here have the ability to produce continuous and differentiable solutions which satisfy the governing equation(s) exactly. Under many circumstances, they can provide helpful insights into ground water-surface water exchanges in 2-D and 3-D [19]. These powerful tools (e.g., series solutions, separation of variables, Laplace and Hankel transforms, etc.) can be augmented with a simple numerical technique such as weighted least squares minimization (WLS) or numerical inversion to address more geometrically or mathematically complex fully saturated or saturated–unsaturated flow problems [16–24]. Yeh and Chang [24] recently presented a review on analytical and semi-analytical techniques applied to simulate saturated–unsaturated flow in a pumping test. The resulting semi-analytical approaches satisfy mass balance and boundary conditions accurately. To date, researchers have used semi-analytical schemes to independently address the free boundary saturated–unsaturated steady flow in homogenous systems [25] and topography-driven

* Corresponding author. Tel.: +1 5198884567x38864.
E-mail address: aaameli@uwaterloo.ca (A.A. Ameli).

saturated flow in heterogeneous aquifers with geometrically complex stratification [18]. However, these issues have never been addressed concurrently. In addition, a robust regional subsurface model requires consideration of the interaction between subsurface flow and the topographic surface. Existing semi-analytical models have paid scarce attention to this issue, and also have neglected the capillary fringe zone [22,23,25]. However, researchers have experimentally and numerically shown that horizontal flow in this zone can have an effect on the magnitude of subsurface flow toward a stream and upon the water table location [2,26].

Multiple researchers have applied semi-analytical series solutions method to simulate topography-controlled saturated steady flow in unconfined aquifers [17,18]. The series solution method is a mesh-free scheme and is able to handle free boundary problems without mesh generation issues. The solutions satisfy continuity of mass exactly over both the saturated and vadose zones. Boundary and continuity conditions along interfaces are satisfied accurately, and explicit and continuous error estimates are immediately available. To simulate the vadose zone using the series solution method, the pressure head-hydraulic conductivity relationship is described using the exponential Gardner model [27]. Pullan [28] has demonstrated that this exponential model is acceptable for a wide range of soils.

3. Problem statement

Fig. 1 shows the general schematic of a stratified soil profile that can be modeled using methods derived herein. An aquifer with length L is subdivided into M layers with arbitrary geometry, each with saturated conductivity K_m^s. Layers are indexed downward from $m = 1$ to $m = M$ and are bounded by the curve $z_m(x)$ above and $z_{m+1}(x)$ below. The bottom bedrock $z_{M+1}(x)$ and sides of the aquifer are impermeable. The topographic surface ($z_1(x)$) is subject to a specified surface flux distribution function (which may be calculated from rainfall, evaporation and transpiration) and/or a Dirichlet condition along surface water bodies (e.g., a river with

specified width and head). These conditions are easily amended to account for the presence of multiple surface water features. The saturated–unsaturated interface or top of capillary fringe ($z_{cf}(x)$) is a moving boundary which defines the location of the top of the saturated zone and the bottom of unsaturated zone. The water table is defined as a boundary with zero pressure head. All layer interfaces, the topographic surface, and the bedrock surface are specified prior to solution.

Here the M-Layer system is divided into two zones: the saturated zone (with M_s layers) and unsaturated zone (with M_u layers). The relationship between M, M_s and M_u is a priori unknown and will be discerned through the solution of the problem, since the top of capillary fringe might intersect multiple layers. Note that hereafter (s) and (u) describe saturated and unsaturated properties/variables.

For the saturated zone the problem is posed in terms of a discharge potential, ϕ_m^s [L^2T^{-1}], defined as

$$\phi_m^s = K_m^s h_m(x, z) \tag{1}$$

where $h_m(x, z)$ is the total hydraulic head in layer m, and K_m^s is the saturated hydraulic conductivity of the mth layer [LT^{-1}]. Using continuity of mass and Darcy's law, each saturated layer's discharge potential function must satisfy the Laplace equation:

$$\frac{\partial^2 \phi_m^s}{\partial x^2} + \frac{\partial^2 \phi_m^s}{\partial z^2} = 0 \quad \text{for } m = M^*, \ldots, M \tag{2}$$

where M^* is the uppermost layer where the top of capillary fringe interface (z_{cf}) exists. For the vadose zone, the problem is expressed in terms of a Kirchhoff potential ϕ_m^u [L^2T^{-1}] in a manner similar to [27,29]. The Kirchhoff potential is a function of pressure head φ [L]

$$\phi_m^u(\varphi_m) = \int_{-\infty}^{\varphi_m} K_m(\eta) d\eta \tag{3}$$

and the gradient of this potential corresponds to the flow rate in the mth unsaturated layer. Using the exponential Gardner model with air entry pressure (as originally included by Rijtema [30])
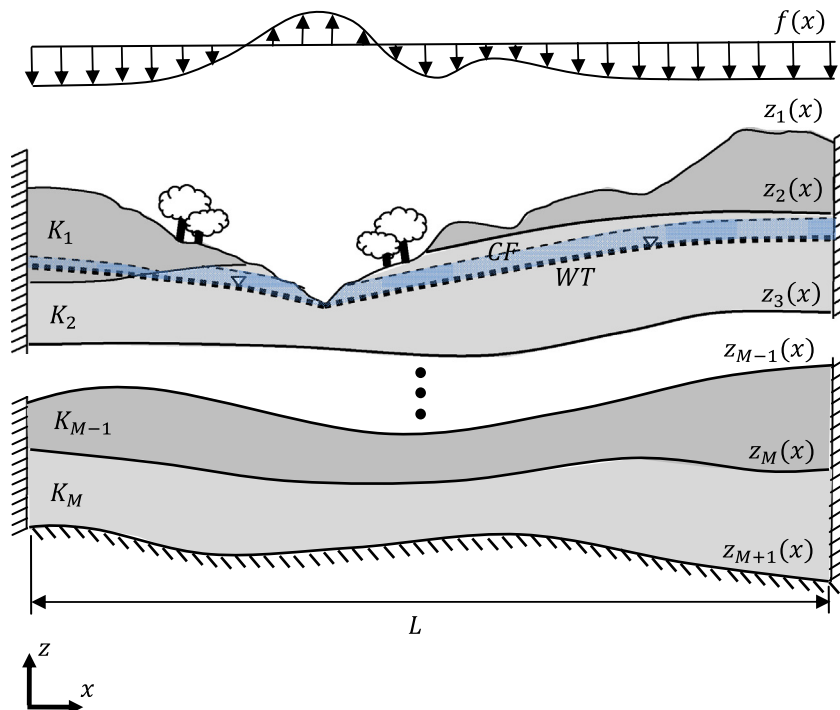

Fig. 1. Layout of the general problem. M layers are separated by the interfaces $z_m(x)$, with $z_{M+1}(x)$ corresponding to the bottom bedrock and $z_1(x)$ corresponding to the topographic surface. CF refers to the boundary between saturated and unsaturated zones.

$$K_m(\varphi_m) = K_m^s \exp(\alpha_m(\varphi_m - \varphi_m^e)) \tag{4}$$

for each unsaturated layer, the Kirchhoff potential is:

$$\phi_m^u(\varphi_m) = \frac{K_m^e}{\alpha_m} \exp(\alpha_m \varphi_m) \tag{5}$$

where $K_m^e = K_m^s \exp(-\alpha_m \varphi_m^e)$ [LT^{-1}], α_m [L^{-1}] is sorptive number and φ_m^e [L] is the air entry pressure head of the mth layer respectively. Using the Kirchhoff potential and Gardner soil characteristic model, the non-linear steady-state form of Richards' equation,

$$\frac{\partial}{\partial x}\left(K_m(\varphi_m)\frac{\partial \varphi_m}{\partial x}\right) + \frac{\partial}{\partial z}\left(K_m(\varphi_m)\frac{\partial \varphi_m}{\partial z}\right) + \frac{\partial}{\partial z}K_m(\varphi_m) = 0 \tag{6}$$

is simplified to an equivalent linear 2-D governing equation for each layer of the vadose zone [27,31,32]:

$$\frac{\partial^2 \phi_m^u}{\partial x^2} + \frac{\partial^2 \phi_m^u}{\partial z^2} + \alpha_m \frac{\partial \phi_m^u}{\partial z} = 0 \quad \text{for } m = 1, \dots, M_u \tag{7}$$

For both unsaturated and saturated 2-D steady flow, the stream function formulation will be useful for applying some of the continuity and boundary conditions. The stream function formulation can be obtained using a generalized form of the Cauchy-Riemann equations for unsaturated flow [33],

$$\frac{\partial \psi_m^u}{\partial x} = -\frac{\partial \phi_m^u}{\partial z} - \alpha_m \phi_m^u \quad \text{and} \quad \frac{\partial \psi_m^u}{\partial z} = \frac{\partial \phi_m^u}{\partial x} \quad \text{for } m = 1, \dots, M_u \tag{8}$$

and Cauchy–Riemann equations for saturated flow,

$$\frac{\partial \psi_m^s}{\partial x} = -\frac{\partial \phi_m^s}{\partial z} \quad \text{and} \quad \frac{\partial \psi_m^s}{\partial z} = \frac{\partial \phi_m^s}{\partial x} \quad \text{for } m = M^*, \dots, M \tag{9}$$

where ψ_m^u and ψ_m^s are unsaturated and saturated stream function of the mth layer respectively. The unsaturated and saturated governing equations are equivalent to the following equations in terms of the stream function for each layer of unsaturated and saturated zones:

$$\frac{\partial^2 \psi_m^u}{\partial x^2} + \frac{\partial^2 \psi_m^u}{\partial z^2} + \alpha_m \frac{\partial \psi_m^u}{\partial z} = 0 \quad \text{for } m = 1, \dots, M_u \tag{10}$$

$$\frac{\partial^2 \psi_m^s}{\partial x^2} + \frac{\partial^2 \psi_m^s}{\partial z^2} = 0 \quad \text{for } m = M^*, \dots, M \tag{11}$$

In a manner similar to Read and Broadbridge [33] for the vadose zone and Wong and Craig [18] for the saturated zone, the normal first order derivatives along a layer interface and the capillary fringe surface can be decomposed into vertical and horizontal components when the cosine of the slope angle describing each evaluation curve approximated as unity. The resulting equations for unsaturated and saturated zones are as follows:

$$\frac{\partial \phi_m^u}{\partial \eta} = \frac{\partial \phi_m^u}{\partial z} - \frac{d\hat{z}}{dx}\frac{\partial \phi_m^u}{\partial x} + \alpha_m \phi_m^u \tag{12}$$

$$\frac{\partial \phi_m^s}{\partial \eta} = \frac{\partial \phi_m^s}{\partial z} - \frac{d\hat{z}}{dx}\frac{\partial \phi_m^s}{\partial x} \tag{13}$$

where η is the coordinate normal to each interface represented by the function $\hat{z}(x)$, which is either a layer interface $z_m(x)$ or top of capillary fringe $z_{cf}(x)$. Using the above equations (Eqs. (12) and (13)) and Cauchy–Riemann equations (Eqs. (8) and (9)) the boundary and continuity conditions along unsaturated and saturated interfaces can be represented in terms of either potential or stream function.

Across the sides of the domain in both unsaturated and saturated zones, no-flow conditions in x-direction are imposed. The stream function equivalent formulas for unsaturated and saturated zones used in current paper are:

$$\psi_m^u(0, z) = 0 \quad \text{for } m = 1, \dots, M_u \tag{14a}$$

$$\psi_m^u(L, z) = 0 \quad \text{for } m = 1, \dots, M_u \tag{14b}$$

$$\psi_m^s(0, z) = 0 \quad \text{for } m = M^*, \dots, M \tag{15a}$$

$$\psi_m^s(L, z) = 0 \quad \text{for } m = M^*, \dots, M \tag{15b}$$

where L is the length of the domain (Fig. 1). The topographic surface boundary condition with the arbitrary infiltration-evapotranspiration function $f(x)$ [LT^{-1}] is:

$$\frac{\partial \phi_1^u}{\partial \eta}(x, z_1(x)) = f(x) \tag{16a}$$

or, using the stream function formulation as done in this paper:

$$\frac{\partial \psi_1^u}{\partial x} + \frac{dz_1(x)}{dx}\frac{\partial \psi_1^u}{\partial z} = -f(x) \tag{16b}$$

where $f(x)$ is taken as positive for infiltration and negative for evapotranspiration. Along surface water features a uniform hydraulic head is applied. The continuity of flux along the vadose zone layers interfaces for $m = 2, \dots, M_u$ can be represented as its stream function equivalent:

$$\psi_m^u(x, z_m(x)) = \psi_{m-1}^u(x, z_m(x)) \tag{17}$$

Similarly, the continuity of head φ^u along vadose zone interfaces in terms of the Kirchhoff potential is

$$\frac{1}{\alpha_m}\ln\left(\frac{\alpha_m \phi_m^u}{K_m^s}\right) = \frac{1}{\alpha_{m-1}}\ln\left(\frac{\alpha_{m-1}\phi_{m-1}^u}{K_{m-1}^s}\right) \tag{18}$$

For the saturated zone, the continuity of flux (in terms of stream function) and pressure head (in terms of discharge potential) along each saturated layer interface (for $m = M^* + 1, \dots, M$) can be represented as:

$$\psi_m^s(x, z_m(x)) = \psi_{m-1}^s(x, z_m(x)) \tag{19}$$

$$\frac{\phi_m^s(x, z_m(x))}{K_m^s} = \frac{\phi_{m-1}^s(x, z_m(x))}{K_{m-1}^s} \tag{20}$$

No-flow conditions are imposed at the bottom of the domain (bedrock) in the saturated zone which can be also represented in terms of stream function as:

$$\psi_M^s(x, Z_{M+1}(x)) = 0 \tag{21}$$

To complete the problem statement, continuity of flux and pressure head must be enforced along the boundary between unsaturated and saturated zones, here referred to as the top of capillary fringe (cf):

$$\psi_m^u(x, z_{cf}^-(x)) = \psi_m^s(x, z_{cf}^+(x)) \tag{22}$$

$$\frac{\phi_m^s}{K_m^s}(x, z_{cf}^+(x)) - z_{cf}^+(x) = \varphi_m^u(x, z_{cf}^-(x)) = \varphi_m^e \tag{23}$$

here m is the layer where top of capillary fringe is located. In each unsaturated layer ($M = 1, \dots, M_u$), the general stream function solution of the following form is assumed:

$$\psi_m^u(x, z) = \sum_{n=0}^{N} A_{nm}[\sin(\omega_n x)\exp(\gamma_{nm}z)] + B_{nm}[\sin(\omega_n x) \\ \times \exp(\bar{\gamma}_{nm}Z)] \tag{24}$$

Note that the form of this solution is obtained using the method of separation of variables and satisfies the unsaturated governing equation (Eq. (10)). In the preceding equation n represents the coefficient index, N is the order of approximation or total number of terms in the series solution, and A_{nm}, B_{nm} are the series coefficients

associated with the mth unsaturated layer and nth coefficient index. Through judicious selection of ω_n, γ_{nm} and $\bar{\gamma}_{nm}$ the sides no-flow conditions (Eqs. (14a) and (14b)) are satisfied:

$$\omega_n = \frac{n\pi}{L}, \quad \gamma_{nm} = \frac{-\alpha_m}{2} + \frac{1}{2}\sqrt{\alpha_m^2 + \left(\frac{2n\pi}{L}\right)^2},$$

$$\bar{\gamma}_{nm} = \frac{-\alpha_m}{2} - \frac{1}{2}\sqrt{\alpha_m^2 + \left(\frac{2n\pi}{L}\right)^2} \tag{25}$$

The Kirchhoff potential series solution can similarly be obtained:

$$\phi_m^u(x,z) = A_{0m}\exp(-\alpha_m Z) - \sum_{n=1}^{N}\left(\frac{\gamma_{nm}}{\omega_n}A_{nm}[\cos(\omega_n x)\exp(\gamma_{nm}Z)]\right.$$
$$\left. + \frac{\bar{\gamma}_{nm}}{\omega_n}B_{nm}[\cos(\omega_n x)\exp(\bar{\gamma}_{nm}Z)]\right) \tag{26}$$

The series solution of the saturated governing equation (Eq. (11)) in terms of stream function is similarly obtained using the method of separation of variables while C_{nm}, D_{nm} are the saturated series coefficients associated with the mth layer ($m = M^*,\ldots,M$).

$$\psi_m^s(x,z) = \sum_{n=0}^{N}(C_{nm}[\sin(\omega_n x)\exp(\omega_n Z)] + D_{nm}[\sin(\omega_n x)$$
$$\times \exp(-\omega_n Z)]) \tag{27}$$

Again, through judicious selection of $\omega_n = n\pi/L$ for $n = 0,\ldots,N$, the side no-flow conditions (Eqs. (15a) and (15b)) are satisfied. The saturated discharge potential series solution can be obtained using Cauchy–Riemann conditions:

$$\phi_m^s(x,z) = C_{0m} - \sum_{n=1}^{N}(C_{nm}[\cos(\omega_n x)\exp(\omega_n z)]$$
$$+ D_{nm}[\cos(\omega_n x)\exp(-\omega_n z)]) \tag{28}$$

The unknowns coefficients A_{nm}, B_{nm} and C_{nm}, D_{nm} will be calculated to satisfy the continuity and boundary conditions (Eqs. (16)–(23)).

4. Solution

The series solution for above the top of capillary fringe (i.e., the unsaturated zone) and below the top of capillary fringe (i.e., ground water and capillary fringe zones) will be determined separately by minimizing the boundary and continuity condition errors at a set of NC uniformly spaced control points located along each layer interface, the capillary fringe top, the topographic surface, and the bedrock. The location of the top of capillary fringe and water table are unknown priori, and will be obtained through a robust iterative scheme. Initially, the top of capillary fringe is fixed to be equal to the river hydraulic head, and a Dirichlet condition of $\varphi = \varphi_m^e$ (where m is the layer where top of capillary fringe is located) is applied. The unknown coefficients for the potential within the unsaturated zone are then calculated by minimizing the boundary and continuity condition errors at a set of NC control points along each interface within the unsaturated zone (the topographic surface, top of capillary fringe, and layer interfaces), for a total of $NC \times (M_u + 1)$ control points. The total weighted sum of squared errors (TWSSE) is here subdivided into the errors along mentioned evaluation curves, i.e.,

$$TWSSE^u = WSSE_t + \sum_{m=2}^{M_u} WSSE_m + WSSE_{cf} \tag{29a}$$

where

$$WSSE_t = \sum_{i=1}^{NC} w_i\left[\frac{\partial \phi_1^u}{\partial \eta}(x_i, z_1(x_i)) - f(x_i)\right]^2 \tag{29b}$$

$$WSSE_m = \sum_{i=1}^{NC} w_i[\psi_m^u(x_i, z_m(x_i)) - \psi_{m-1}^u(x_i, z_m(x_i))]^2$$
$$+ \sum_{i=1}^{NC} w_i[\varphi_m^u(x_i, z_m(x_i)) - \varphi_{m-1}^u(x_i, z_m(x_i))]^2,$$
$$\text{for } m = 2,\ldots,M_u \tag{29c}$$

$$WSSE_{cf} = \sum_{i=1}^{NC} w_i[\varphi_{cf}^u(x_i, z_{cf}^-(x_i)) - \varphi_{cf}^e]^2 \tag{29d}$$

the subscripts refer to the errors along the topographic surface (t), layer interfaces (m) and top of capillary fringe (cf). By minimizing Eq. (29a), approximations of the unknown unsaturated coefficients (A_{nm}^1, B_{nm}^1) at the first iteration (here the superscript refers to iteration number) will be obtained and the series solutions for stream function (24) and Kirchhoff potential (26) are fully defined. This intermediate unsaturated zone solution provides the flux or stream function distribution along the capillary fringe, which acts as the top boundary condition in the solution of the saturated zone problem (Eq. (22)). In a manner similar to the unsaturated zone, the saturated unknown coefficients are calculated by minimizing the total weighted sum of squared error (TWSSE) at a set of control points along top of capillary fringe location, bottom bedrock and interfaces between saturated layers.

$$TWSSE^s = WSSE_{cf} + \sum_{m=M^*+1}^{M} WSSE_m + WSSE_b \tag{30a}$$

where

$$WSSE_{cf} = \sum_{i=1}^{NC} w_i[\psi_m^s(x_i, z_{cf}^+(x_i)) - \psi_m^u(x_i, z_{cf}^-(x_i))]^2 \tag{30b}$$

Here m is the layer where top of capillary fringe is located

$$WSSE_m = \sum_{i=1}^{NC} w_i[\psi_m^s(x_i, z_m(x_i)) - \psi_{m-1}^s(x_i, z_m(x_i))]^2$$
$$+ \sum_{i=1}^{NC} w_i\left[\frac{\phi_m^s}{K_m^s}(x_i, z_m(x_i)) - \frac{\phi_{m-1}^s}{K_{m-1}^s}(x_i, z_m(x_i))\right]^2 \tag{30c}$$

$$WSSE_b = \sum_{i=1}^{NC} w_i[\psi_M^s(x_i, z_{M+1}(x_i))]^2 \tag{30d}$$

By minimizing Eq. (30a), an approximation of the unknown saturated coefficients (C_{nm}^1, D_{nm}^1) is obtained and the series solution in terms of stream function (27) and discharge potential (28) are fully defined. The saturated series solution provides a water pressure distribution along the approximate top of capillary fringe surface at each control point $(\varphi_{cf}^1(x_i))$. In each iteration, this may be used to modify top of capillary fringe location according to:

$$z_{cf}^{k+1}(x_i) = z_{cf}^k(x_i) + \tau(\varphi_{cf}^k(x_i) - \varphi_m^e) \tag{31}$$

where k is the iteration number, φ_m^e is the air entry pressure head of the mth layer (m is the layer where top of capillary fringe is located), and τ is a relaxation factor. The top of capillary fringe location is therefore revised and this iteration scheme will be continued until the saturated pressure head at each control points along top of capillary fringe $\varphi_{cf}^k(x_i)$ converges to air entry pressure. After the location of the top of capillary fringe converges to a fixed position, the water table elevation is obtained as the contour with zero pressure head. Note that solution of the overdetermined system of equations is handled using the LSCOV function of MATLAB.

5. Analysis

The following section describes a set of tests used to demonstrate the quality and the convergence behaviour of the series solutions. The efficiency of the approach is assessed for geometrically complex homogenous and stratified unconfined aquifers under different surface boundary conditions. Normalized continuity and boundary condition errors (Eqs. (32)) are assessed along each interface (m) at points located between the control points used within the least squares solution:

$$\varepsilon_m^{flux}(x_i) = \frac{\left| \frac{\partial \phi^-}{\partial \eta}(x_i) - \frac{\partial \phi^+}{\partial \eta}(x_i) \right|}{\max(f(x)) - \min(f(x))} \quad \text{for } m = 1, \ldots, M+1 \quad (32a)$$

$$\varepsilon_m^{head}(x_i) = \frac{\left| \varphi_{(x_i)}^- - \varphi_{(x_i)}^+ \right|}{\max(\varphi) - \min(\varphi)} \quad \text{for } m = 2, \ldots, M \quad (32b)$$

Note that for the topographic surface (m = 1), $\varepsilon_1^{flux}(x_i)$ is

$$\varepsilon_1^{flux}(x_i) = \frac{\left| f(x_i) - \frac{\partial \phi^+}{\partial \eta}(x_i) \right|}{\max(f(x)) - \min(f(x))}$$

and for the bottom bedrock (m = M + 1):

$$\varepsilon_{M+1}^{flux}(x_i) = \frac{\left| \frac{\partial \phi^-}{\partial \eta}(x_i) \right|}{\max(f(x)) - \min(f(x))}$$

$\min(f(x))$ and $\max(f(x))$ $[LT^{-1}]$ refer to minimum and maximum flux applied across the topographic surface, $\max(\varphi)$ and $\min(\varphi)$ [L] are the maximum and minimum value of the pressure head in the entire domain. In addition, with a manner similar to [25] total root mean square normalized flux error (rmse^{flux}) and total root mean square normalized head error (rmse^{head}) are obtain as follows:

$$\text{rmse}^{flux} = \frac{1}{\sqrt{NC}} \sqrt{\left[\sum_{i=1}^{NC} (\varepsilon_1^{flux}(x_i))^2 + \sum_{i=1}^{NC} (\varepsilon_{M+1}^{flux}(x_i))^2 + \sum_{i=1}^{NC} (\varepsilon_m^{flux}(x_i))^2 \right]}$$
$$(33a)$$

$$\text{rmse}^{head} = \frac{1}{\sqrt{NC}} \sqrt{\left[\sum_{i=1}^{NC} (\varepsilon_m^{head}(x_i))^2 \right]} \quad \text{for } m = 2, \ldots, M \quad (33b)$$

The rate of convergence of the solutions with a free boundary condition will also be assessed in the below cases.

5.1. Example 1: homogenous system

The configuration for a hypothetical homogenous unconfined aquifer system adjacent to a 20 m wide river is shown in Fig. 2. Fig. 2(a) shows the infiltration and evapotranspiration function (f(x)) applied across the topographic surface. The hydrological and hydrogeological parameters used in example 1 are: $K^s = 1 \text{ m d}^{-1}$, $\alpha = 0.5 \text{ m}^{-1}$, $\varphi^e = -0.5 \text{ m}$, River Head = 5.5 m, River Width = 20 m.

The flow net for this problem, along with the calculated top of capillary fringe and water table locations are shown in Fig. 2(b). This solution was identified after 10 iterations. Hydraulic head contours in the saturated zone show that conditions are nearly hydrostatic beneath the water table.

The solution was obtained using $(M_u + M_s)(2N + 1) = 282$ coefficients and 1400 control points along each evaluation curve (i.e., the topographic surface, bedrock and top of capillary fringe). The topographic surface boundary condition (Eq. (16b)), no-flow bedrock boundary condition (Eq. (21)) and continuity of flux (Eq. (22)) and head (Eq. (23)) across top of capillary fringe, have been satisfied by expanding the general series solution (Eqs. (24), (26), (27), and (28)) at control points along each interface and minimizing error using weighted least square method (Eqs. (29) and (30)). Note that since the units and magnitude of the flux and head errors are different, weighting coefficients for each control point (w_i) were considered as 4 and 1 for flux and head conditions respectively. A relaxation factor $\tau = 0.5$ used to control the convergence behaviour of the top of the capillary fringe (Eq. (31)).

Fig. 3 demonstrates the quality and the convergence behaviour of the series solutions used in example 1. Fig. 3(a) shows the convergence of the solution as the pressure head at 1400 control points along the free boundary top of capillary fringe converges to air entry pressure ($\varphi^e = -0.5$ m). As can be seen from the figure, control points along the intersection of the top of capillary fringe and topographic surface have the largest absolute error at initial iterations. Fig. 3(b) shows the normalized flux errors across the topographic surface (ε_1^{flux}) and the bottom bedrock (ε_{M+1}^{flux}) at 1400 points between the control points used for least squares minimization.

Although there is a flux error across the impermeable bedrock, the net normalized flux error is on the order 10^{-17}, which guaran-
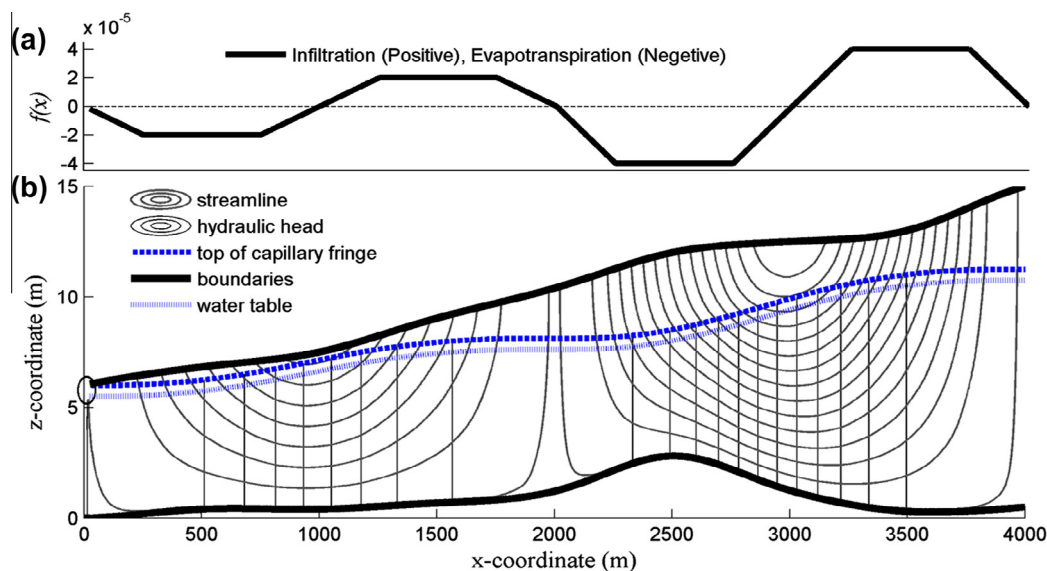

Fig. 2. (a) Surface flux distribution function f(x) used in example 1, (b) layout of the flow streamlines (grey), hydraulic head lines (black), capillary fringe top and water table in a homogenous unconfined aquifer adjacent to a constant head river (left side) after 10 iterations. The river is shown at the left side of the domain.
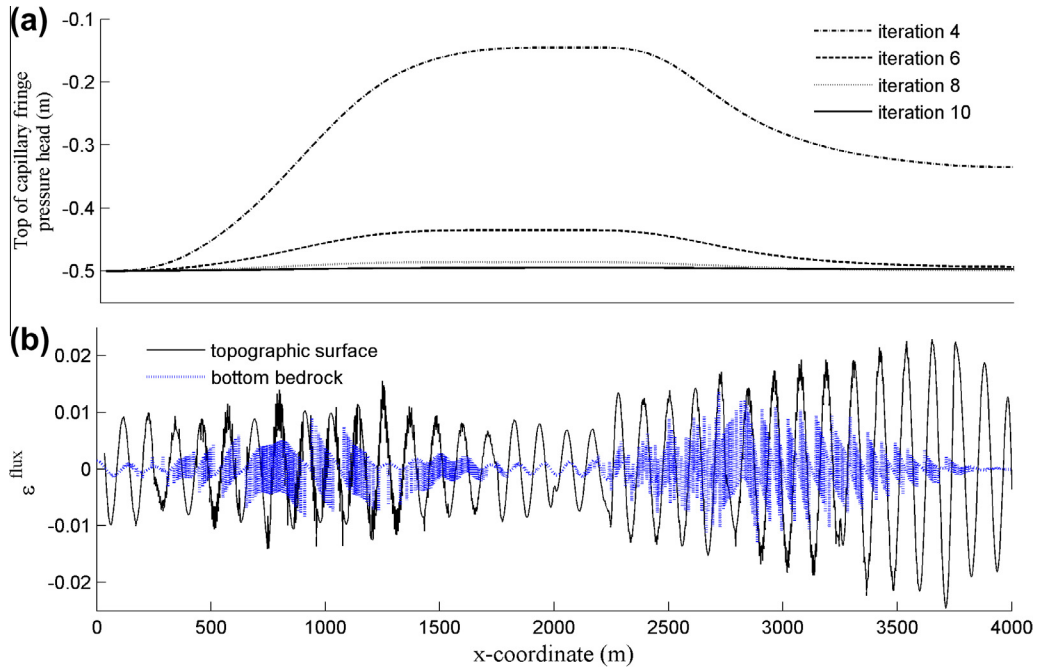
Fig. 3. (a) Convergence of the pressure head along the top of the capillary fringe to air entry pressure ($\varphi^e = -0.5$ m using a relaxation factor of $\tau = 0.5$, (b) Normalized flux error across the topographic surface and the bottom bedrock.

tees mass conservation inside the domain. The largest normalized flux error over both interfaces (2%) occurs along the intersection of the top of capillary fringe and the topographic surface, and on the right side of the topographic surface with higher $f(x_i)$ (Fig. 3(b)). The error along the topographic surface can result from abrupt changes of surface function (evapotranspiration to infiltration and vice versa) that cause Gibbs phenomenon. Although a linear transition was used between infiltration and evapotranspiration (Fig. 2(a)), some degree of function smoothing could have reduced this error. Normalized head errors along the river boundary condition are also on the order 10^{-8} (not shown here). In addition, total root mean square normalized flux error ($rmse^{flux}$) along the topographic surface and bottom bedrock are on the order of 10^{-3}. Note that, since the governing equation is elliptic and satisfied exactly using series solutions method, the largest errors in the domain occur along the system boundaries.

The series solution is seen to be valid and successful (with acceptable ranges of error along boundaries) in naturally complex homogenous regional unconfined aquifer as long as Gibbs phenomenon is avoided and the Fourier series converges.

5.2. Example 2: heterogeneous system

In a second example, a hypothetical regional aquifer system with 4 layers is considered. The 5 m wide river with constant head equal to 10 m is located at the left of the domain. Two different surface flux distributions ($f(x)$) are considered in example 2 to assess the impact of the surface water boundary upon the efficiency of the approach (Fig. 4). The hydrological and hydro-geological parameters used are: $K_1^s = 10$ m d^{-1}, $K_2^s = 8$ m d^{-1}, $K_3^s = 0.8$ m d^{-1}, $K_4^s = 0.08$ m d^{-1}, $\alpha = 1.5$ m^{-1}, (identical for 4 layers), $\varphi^e = -0.25$ m, (identical for 4 layers), River Head = 5 m, River Width = 10 m. The sorptive number (α) and air entry pressure (φ^e) are assumed to be identical for all layers. This assumption guarantees that the continuity of head condition across the layer interfaces in the unsaturated zone (Eq. (18)) can be expressed as a linear equation with respect to the unknown solution coefficients.

Fig. 5 shows the layout of flow net for the two cases. As can be seen, while M is equal to 4 in both cases, M_u and M_s are 2 in case a and for case b due to the intersection of the top of capillary fringe
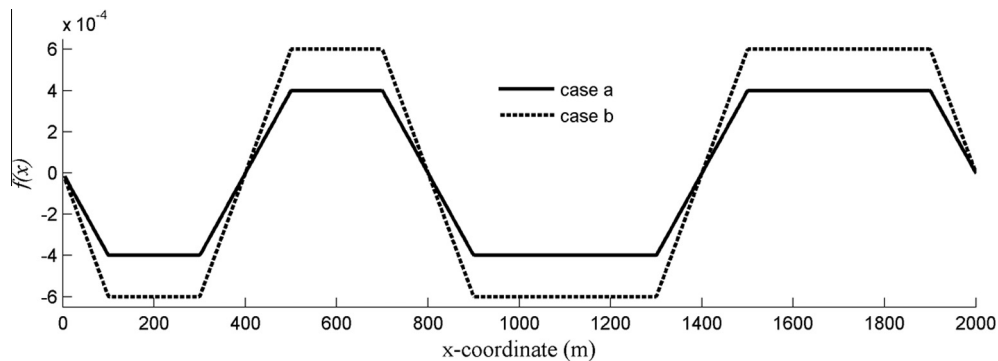

Fig. 4. Surface flux distribution function ($f(x)$) used in example 2, for cases a and b.
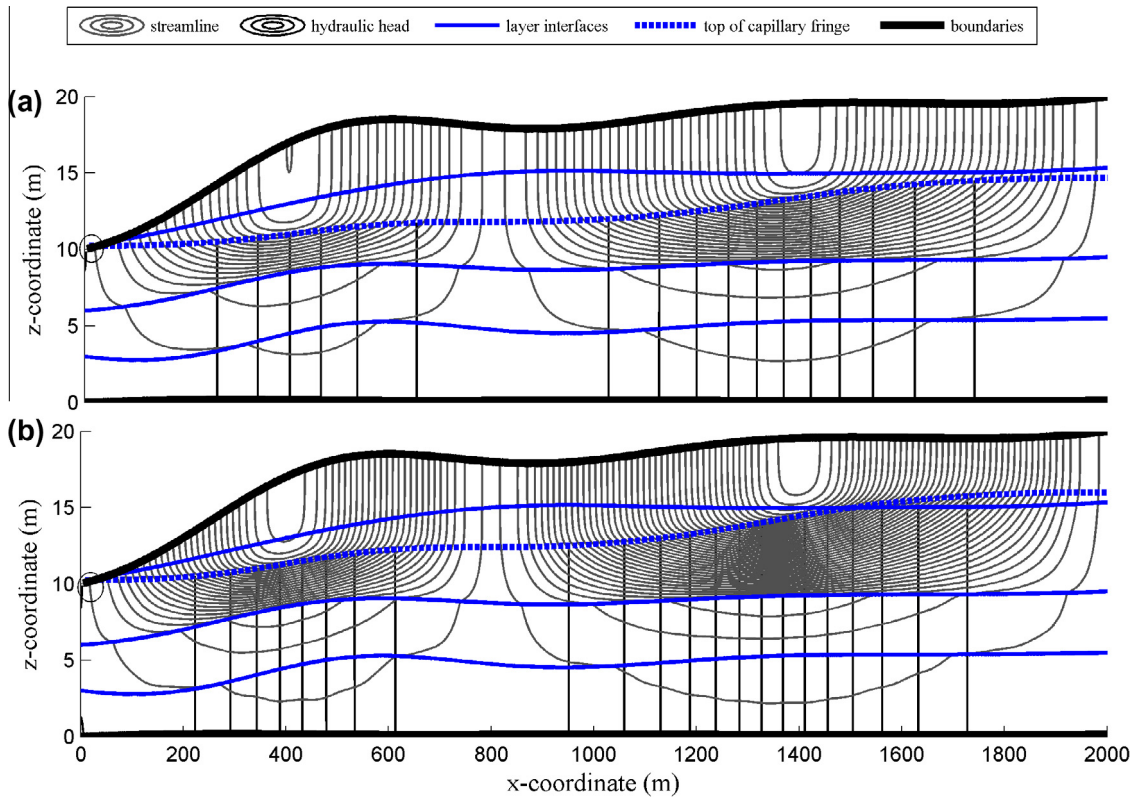
Fig. 5. Layout of flow net in the 4-layer aquifer after 14 iterations, (a) case a, (b) case b. The river is shown at the left side of the domain.

with the first layer interface M_u is 2 and M_s is 3. Fig. 5(b), in addition, demonstrates as infiltration rate increases at $x = 1400$ m, the top of capillary fringe elevation increases and intersects the layer interface.

Note that M^* (the uppermost layer in which the top of capillary fringe is located) is the second and first layer for cases a and b, respectively. The solutions were obtained using $(2N + 1) = 101$ coefficients in each layer $((M_u + M_s)(2N + 1)$ coefficients in total,
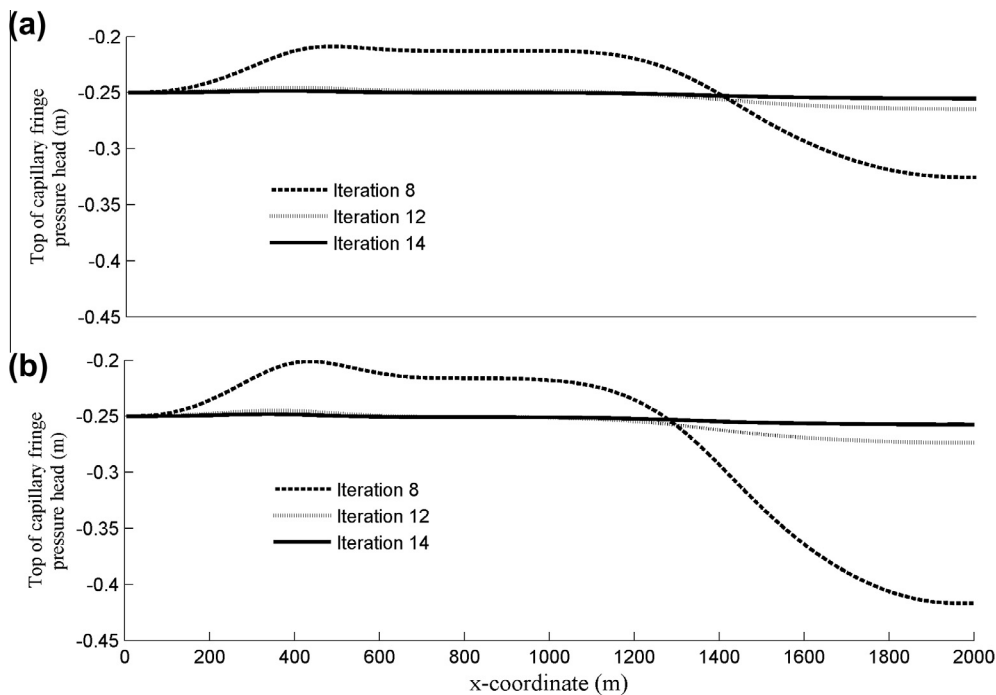

Fig. 6. Convergence of the moving boundary between saturated and unsaturated zones in example 2; (a) case a with relaxation factor $(\tau) = 0.5$, (b) case b with relaxation factor $(\tau) = 0.375$.

404 for case a and 505 for case b), and 1200 control points along each evaluation curve.

Similar to example 1, for test case a each control point weighting coefficients (w_i) has been considered as 4 and 1 for flux and head boundaries respectively and the relaxation factor (τ) equal to 0.5 used for the top of capillary fringe pressure head convergence (Eq. (31)). For case b, on the other hand, a smaller relaxation factor (τ) = 0.375 was required to handle complications due to the intersection of the top of capillary fringe and the layer interface. Fig. 6 shows the rapid convergence of the solution for cases a and b while the pressure head at 1200 control points along the top of capillary fringe free boundary converges to the air entry pressure ($\varphi^e = -0.25$ m).

The steepness of the capillary fringe surface around the intersection combined with the change in material properties along this free boundary interface may cause Gibbs phenomenon in case b; this describes the slower convergence rate of the control points around the intersection Fig. 7 shows the normalized flux errors across the top ε_m^{flux} and the bottom ε_{M+1}^{flux} boundary conditions, and along the layer interfaces ε_m^{flux} at 1200 points for both cases .The maximum normalized flux errors across all the interfaces are on the order of 10^{-2} m d^{-1}. For both cases, the maximum normalized

flux error along the topographic surface (2%) occurs at sharp changes in surface function $f(x)$ (Fig. 4). A high contrast in hydraulic conductivity ($K_s^2/K_s^3 = 10$) across 2nd interface z_3 (the interface between the second layer and the third one), could cause normalized flux error as high as 2% for both cases. Intersection of the top of capillary fringe with the first layer interface (z_2) caused an abrupt change in the governing equation from the unsaturated into the saturated along this interface. Consequently, normalized continuity flux errors across the first layer interface (z_2) in case b are higher than in case a around the intersection with a maximum error of 3% at $x = 1500$ m (the intersection point circle in Fig. 7(b)). Normalized flux error trend across this interface for case b are almost identical to case a for points far away from the intersection. In addition, for both cases a and b total root mean square normalized flux error (rmse^{flux}) are on the order of 10^{-3}, with the largest contribution to this error found along the topographic surface.

The errors in flux are within acceptable range, although the previous series solutions of [18,25] reported lower flux errors. This may be attributed to the discontinuities in the gradient of the infiltration distribution function, the complexity of the stratified domain geometry, or the complexity of the free boundary problem, any of which can exacerbate Gibbs phenomenon. However, the
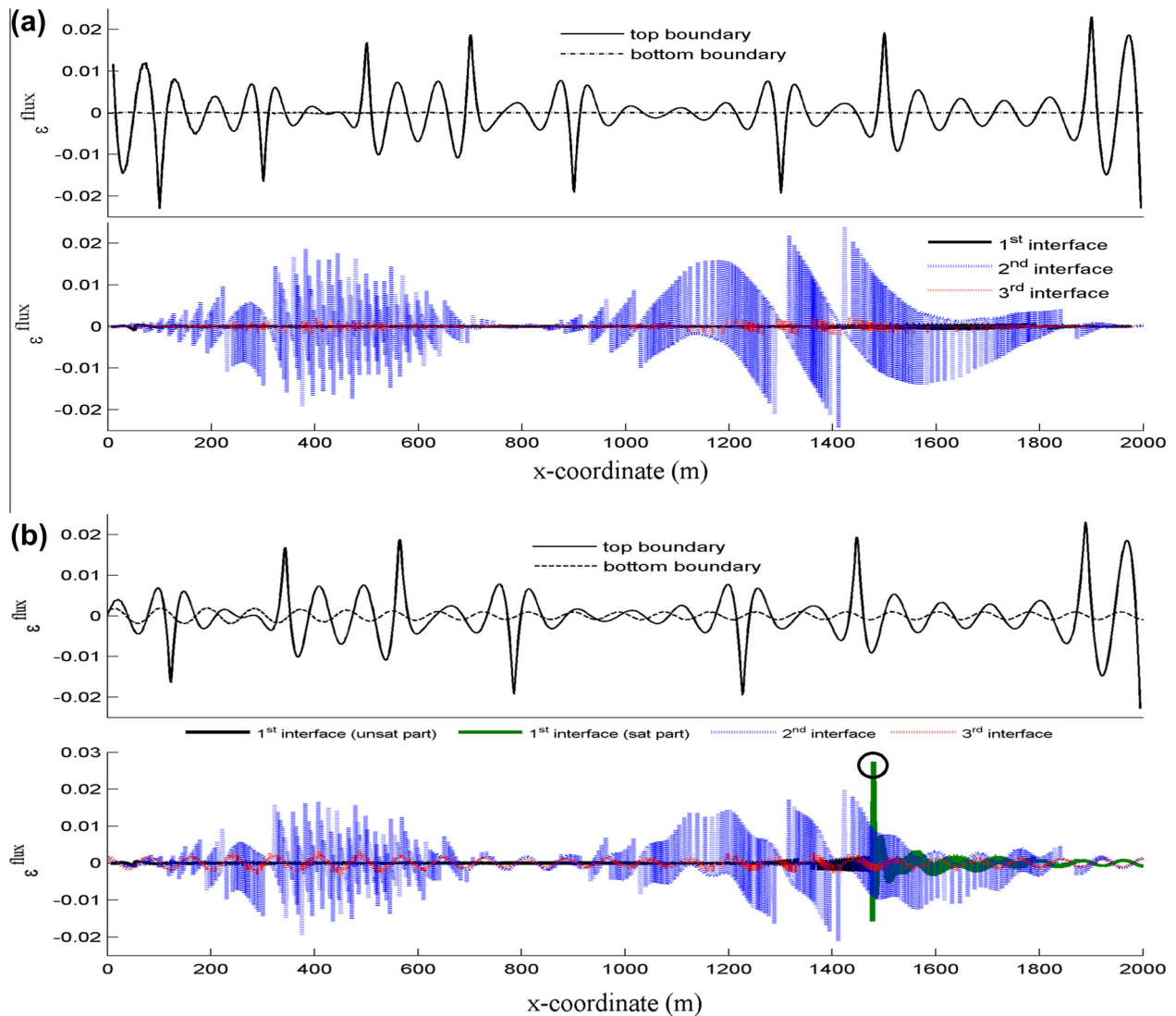

Fig. 7. Normalized flux boundary and continuity error across internal interfaces (1200 points) after 14 iterations in the example 2; (a) case a, (b) case b. The unsaturated and saturated parts of the first layer interface (z_2) are shown in separate colours (black and green respectively) and black circle shows the location of the maximum error along z_2. (For interpretation of the references to colour in this figure legend, the reader is referred to the web version of this article.)
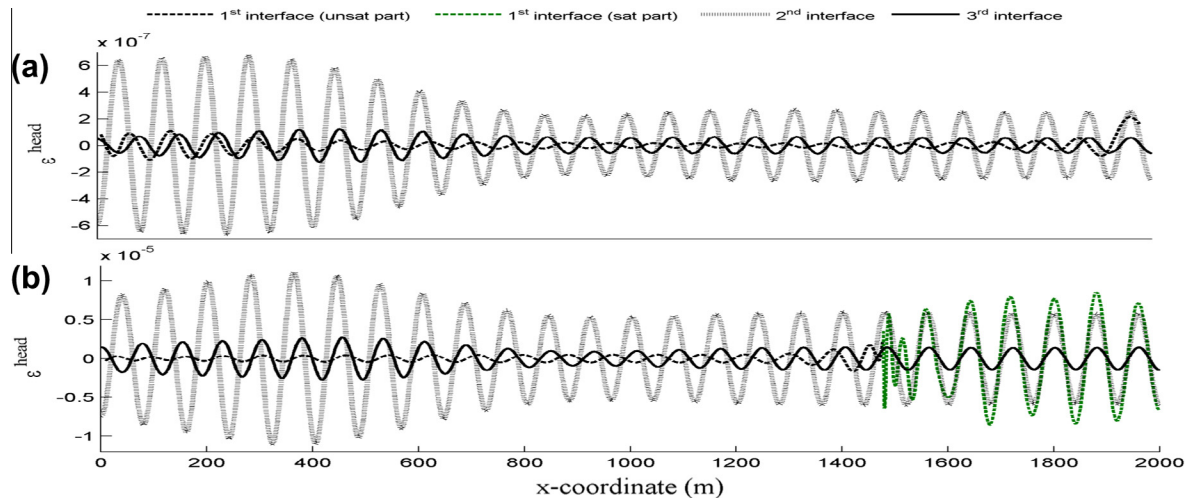
Fig. 8. Normalized head continuity error across internal interfaces in example 2, (a) case a, (b) case b. The unsaturated and saturated part of the first layer interface (z_2) are shown in separate colours (black and green respectively). (For interpretation of the references to colour in this figure legend, the reader is referred to the web version of this article.)

net normalized flux error across layer interfaces and bottom bed-rock are on the order of 10^{-18} to 10^{-14} for both cases except for the first layer interface in case b with errors on the order of 10^{-7} (due to intersection of the top of capillary fringe with the first layer interface). Fig. 8 illustrates the normalized head errors ε_m^{head} across the layer interfaces at 1200 points for both cases. Similar to the flux errors across the layer interfaces, for case b the maximum normalized head errors across the first layer interface occur at the intersection of the top of capillary fringe and this interface that is in a magnitude of 10^{-5} (m). For both cases, a high contrast in hydraulic conductivity (8/0.8) across 2nd interface (z_3) could cause the highest normalized head errors over the entire domain. In addition, for both cases a and b total root mean square normalized head error (rmse^{head}) are on the order of 10^{-7}.

Despite the presence of complex geometry and stratification, the presence of a free boundary the series solution approach can still be deemed successful for the simulation of steady saturated–unsaturated flow induced by surface water bodies in naturally complex regional homogenous and stratified hillslopes as long as the Fourier series converges. This is contingent upon

• The continuity conditions being linear (e.g., identical sorptive number and air entry pressure head for all unsaturated layers)
• interfaces being continuous in value and gradient
• the surface function ($f(x)$) being continuous in value and ideally gradient

6. Conclusion

Mixed saturated–unsaturated flow simulation has historically not been within the reach of analytical schemes, particularly in geo-metrically complex heterogeneous aquifers. In this paper, robust general solutions for free boundary steady saturated–unsaturated flow in naturally complex heterogeneous geological settings have been developed and assessed. The capillary fringe zone has been considered as a distinctive zone with free boundary at the top and bottom. Semi-analytical series solutions have been showed to sim-ulate coupled saturated and unsaturated flow accurately (as long as Gibbs phenomenon issue has been addressed) with acceptable rates of convergence and errors in top of capillary fringe and water table locations. Without discretization artefacts, introduced by numerical schemes, boundary errors, pressure head, flux and stream function distributions are immediately available as continuous function of

the space. The number of degrees of freedom required to simulate these relatively complex systems is small.

Demonstrated efficiency of the pseudo-linear approach sug-gests that it is worth considering to later extend the series solution to transient and 3-D problems while considering more challenging cases (such as when sorptive number and air entry pressure vary between different aquifer layers).

References

[1] Jyrkama MI, Sykes JF. Sensitivity and uncertainty analysis of the recharge boundary condition. Water Resour Res 2006;42(1):W01404. http://dx.doi.org/10.1029/2005WR004408.
[2] Romano CG, Frind EO, Rudolph DL. Significance of unsaturated flow and seepage faces in the simulation of steady-state subsurface flow. Ground Water 1999;37:625–32. http://dx.doi.org/10.1111/j.1745-6584.1999.tb01151.x.
[3] Kollet SJ, Maxwell RM. Integrated surface-groundwater flow modeling: a free-surface overland flow boundary condition in a parallel groundwater flow model. Adv Water Resour 2006;29:945–58. http://dx.doi.org/10.1016/j.advwatres.2005.08.006.
[4] Liang H, Guodong L, Xinfeng L, Modeling and predicting groundwater pollution caused by oil pipeline leakage using MODFLOW and MT3D. In: 3rd international conference on bioinformatics and biomedical engineering, ICBBE 2009, Beijing, China.
[5] Odenwald B, Stamm J, Herrling B. Continuous transmissivity transitions for horizontal groundwater flow models. Adv Water Resour 1995;18:257–65. http://dx.doi.org/10.1016/0309-1708(95)00025-E.
[6] Panday S, Huyakorn PS. A fully coupled physically-based spatially-distributed model for evaluating surface/subsurface flow. Adv Water Resour 2004;27:361–82. http://dx.doi.org/10.1016/j.advwatres.2004.02.016.
[7] An H, Ichikawa Y, Tachikawa Y, Shiiba M. Three-dimensional finite difference saturated-unsaturated flow modeling with nonorthogonal grids using a coordinate transformation method. Water Resour Res 2010;46:W11521. http://dx.doi.org/10.1029/2009WR009024.
[8] Knupp P. A moving mesh algorithm for 3-D regional groundwater flow with water table and seepage face. Adv Water Resour 1996;19:83–95. http://dx.doi.org/10.1016/0309-1708(95)00033-X.
[9] Clement TP, Wise WR, Molz FJ. A physically-based, 2-dimensional, finite difference algorithm for modeling variably saturated flow. J Hydrol 1994;161(1–4):71–90. http://dx.doi.org/10.1016/0022-1694(94)90121-X.
[10] Dogan A, Motz LH. Saturated–unsaturated 3D groundwater model. II: verification and application. J Hydrol Eng 2005;10(6):505–15. http://dx.doi.org/10.1061/(ASCE)1084-0699(2005)10:6(505.
[11] Harbaugh A, Banta E, Hill M, McDonald M, MODFLOW-2000, the U.S. Geological Survey modular ground-water model – user guide to

modularization concepts and the ground-water flow process: U.S. Geological Survey Open-File Report 00-92, 2000, 121 p.

[12] Chang Y, Yeh H. Analytical solution for groundwater flow in an anisotropic sloping aquifer with arbitrarily located multiwells. J Hydrol 2007;347:143–52. http://dx.doi.org/10.1016/j.jhydrol.2007.09.012.

[13] Chen J, Tan Y, Chen C. Analytical solutions of one-dimensional infiltration before and after ponding. Hydrol Process 2003;17:815–22. http://dx.doi.org/10.1002/hyp.1202.

[14] Srivastava R, Yeh JTC. Analytical solutions for one-dimensional, transient infiltration toward the water table in homogeneous and layered soils. Water Resour Res 1991;27:753–62. http://dx.doi.org/10.1029/90WR02772.

[15] Yuan F, Lu Z. Analytical solutions for vertical flow in unsaturated, rooted soils with variable surface fluxes. Vadose Zone J 2005;4(4):1210–8. http://dx.doi.org/10.2136/vzj2005.0043.

[16] Craig JR. Analytical solutions for 2D topography-driven flow in stratified and syncline aquifers. Adv Water Resour 2008;31(8):1066–73. http://dx.doi.org/10.1016/j.advwatres.2008.04.011.

[17] Read WW, Volker RE. Series solutions for steady seepage through hillsides with arbitrary flow boundaries. Water Resour Res 1993;29(8):2871–80. http://dx.doi.org/10.1029/93WR00905.

[18] Wong S, Craig JR. Series solutions for flow in stratified aquifers with natural geometry. Adv Water Resour 2010;33(1):48–54. http://dx.doi.org/10.1016/j.advwatres.2009.10.006.

[19] Haitjema HM. Analytic element modeling of groundwater flow. San Diego: Academic Press; 1995.

[20] Craig JR. Analytic elements for flow in harmonically heterogeneous aquifers. Water Resour Res 2009;45(6):WR007800. http://dx.doi.org/10.1029/2009WR007800.

[21] Tartakovsky GD, Neuman SP. Three-dimensional saturated–unsaturated flow with axial symmetry to a partially penetrating well in a compressible unconfined aquifer. Water Resour Res 2007;43(1):W01410. http://dx.doi.org/10.1029/2006WR005153.

[22] Mishra PK, Vesselinov VV, Kuhlman KL. Saturated-unsaturated flow in a compressible leaky-unconfined aquifer. Adv Water Resour 2012;42:62–70. http://dx.doi.org/10.1016/j.advwatres.2012.03.007.

[23] Mishra PK, Neuman SP. Improved forward and inverse analyses of saturated-unsaturated flow toward a well in a compressible unconfined aquifer. Water Resour Res 2010;46:W07508. http://dx.doi.org/10.1029/2009WR008899.

[24] Yeh HD, Chang YC. Recent advances in modeling of well hydraulics. Adv Water Resour 2013;51:27–51. http://dx.doi.org/10.1016/j.advwatres.2012.03.006.

[25] Tritscher P, Read WW, Broadbridge P, Knight JH. Steady saturated–unsaturated flow in irregular porous domains. Math Comput Model 2001;34:177–94. http://dx.doi.org/10.1016/S0895-7177(01)00054-1.

[26] Berkowitz B, Silliman SE, Dunn AM. Impact of the capillary fringe on local flow, chemical migration, and microbiology. Vadose Zone J 2004;3(2):534–48. http://dx.doi.org/10.2136/vzj2004.0534.

[27] Bakker M, Nieber JL. Two-dimensional steady unsaturated flow through embedded elliptical layers. Water Resour Res 2004;40:1–12. http://dx.doi.org/10.1029/2004WR003295.

[28] Pullan AJ. The quasilinear approximation for unsaturated porous media flow. Water Resour Res 1990;26:1219–34. http://dx.doi.org/10.1029/WR026i006p01219.

[29] Philip JR. Seepage shedding by parabolic capillary barriers and cavities. Water Resour Res 1998;34(11):2827–35. http://dx.doi.org/10.1029/98WR01859.

[30] Rijtema PE, Soil moisture forecasting. Technical report nota 513, Instituut voor Cultuurtechniek en Water-huishouding, Wageningen, 1969, 18 p.

[31] Basha HA. Multidimensional quasi-linear steady infiltration toward a shallow water table. Water Resour Res 2000;36(7):1697–705. http://dx.doi.org/10.1029/2000WR900064.

[32] Basha HA. Multidimensional linearized nonsteady infiltration with prescribed boundary conditions at the soil surface. Water Resour Res 1999;35(1):75–83. http://dx.doi.org/10.1029/1998WR900015.

[33] Read W, Broadbridge P. Series solutions for steady unsaturated flow in irregular porous domains. Transp Porous Media 1996;22(2):195–214. http://dx.doi.org/10.1007/BF01143515.